J|A|C|S ARTICLES

Published on Web 08/23/2010

# Understanding the Effect of Magnesium Ion Concentration on the Catalytic Activity of Ribonuclease H through Computation: Does a Third Metal Binding Site Modulate Endonuclease Catalysis?

Ming-Hsun Ho,[†,II] Marco De Vivo,[‡] Matteo Dal Peraro,[*,§] and Michael L. Klein[*,II]

*Department of Chemistry, University of Pennsylvania, 231 South 34th Street, Philadelphia, Pennsylvania, 19104, Department of Drug Discovery & Development, Italian Institute of Technology, Via Morego 30, 16163 Genova, Italy, Institute of Bioengineering, School of Life Sciences, Ecole Polytechnique Fédérale de Lausanne, CH-1015 Lausanne, Switzerland, and Institute of Computational Molecular Science, Temple University, 1900 North 12th Street, Philadelphia, Pennsylvania 19122*

Received April 7, 2010; E-mail: mlklein@temple.edu; matteo.dalperaro@epfl.ch

***Abstract:*** Ribonuclease H (RNase H) belongs to the nucleotidyl-transferase superfamily and hydrolyzes the phosphodiester linkage on the RNA strand of a DNA/RNA hybrid duplex. Due to its activity in HIV reverse transcription, it represents a promising target for anti-HIV drug design. While crystallographic data have located two ions in the catalytic site, there is ongoing debate concerning just how many metal ions bound at the active site are optimal for catalysis. Indeed, experiments have shown a dependency of the catalytic activity on the $Mg^{2+}$ concentration. Moreover, in RNase H, the glutamate residue E188 has been shown to be essential for full enzymatic activation, regardless of the $Mg^{2+}$ concentration. The catalytic center is known to contain two $Mg^{2+}$ ions, and E188 is not one of the primary metal ligands. Herein, classical molecular dynamics (MD) simulations are employed to study the metal−ligand coordination in RNase H at different concentration of $Mg^{2+}$. Importantly, the presence of a third $Mg^{2+}$ ion, bound to the second-shell ligand E188, is a persistent feature of the MD simulations. Free energy calculations have identified two distinct conformations, depending on the concentration of $Mg^{2+}$. At standard concentration, a third $Mg^{2+}$ is found in the catalytic pocket, but it does not perturb the optimal RNase H active conformation. However, at higher concentration, the third $Mg^{2+}$ ion heavily perturbs the nucleophilic water and thereby influences the catalytic efficiency of RNase H. In addition, the E188A mutant shows no ability to engage additional $Mg^{2+}$ ions near the catalytic pocket. This finding likely explains the decrease in catalytic activity of E188A and also supports the key role of E188 in localizing the third $Mg^{2+}$ ion at the active site. Glutamate residues are commonly found surrounding the metal center in the endonuclease family, which suggests that this structural motif may be an important feature to enhance catalytic activity. The present MD calculations support the hypothesis that RNase H can accommodate three divalent metal ions in its catalytic pocket and provide an in-depth understanding of their dynamic role for catalysis.

## Introduction

Ribonuclease (RNase) enzymes belong to the nucleotidyl-transferase (NT) superfamily, which catalyzes the hydrolysis of phosphodiester linkages that form the backbone of RNA strands. Various types of RNase have been identified and grouped into different categories based on the structures and the targeting substrates.[1] Here we focus on RNase H, one of the most important endoribonucleases. The structure and function of RNase H have been extensively studied and characterized through crystallographic and kinetic data.[2−11] Specifically, RNase H is a non-sequence-specific enzyme that cleaves the RNA strand of a DNA/RNA hybrid duplex. It has been found in many species, including viruses, bacteria, and humans,[4,12,13]

[†] University of Pennsylvania.
[‡] Italian Institute of Technology.
[§] Ecole Polytechnique Fédérale de Lausanne.
[II] Temple University.

(1) Worrall, J. A. R.; Luisi, B. F. *Curr. Opin. Struct. Biol.* **2007**, *17*, 128–137.
(2) Katayanagi, K.; Miyagawa, M.; Matsushima, M.; Ishikawa, M.; Kanaya, S.; Ikehara, M.; Matsuzaki, T.; Morikawa, K. *Nature* **1990**, *347*, 306–309.
(3) Nowotny, M.; Gaidamakov, S. A.; Crouch, R. J.; Yang, W. *Cell* **2005**, *121*, 1005–1016.
(4) Nowotny, M.; Gaidamakov, S. A.; Ghirlando, R.; Cerritelli, S. M.; Crouch, R. J.; Yang, W. *Mol. Cell* **2007**, *28*, 264–276.
(5) Nowotny, M.; Yang, W. *EMBO J.* **2006**, *25*, 1924–1933.
(6) Nowotny, M.; Cerritelli, S. M.; Ghirlando, R.; Gaidamakov, S. A.; Crouch, R. J.; Yang, W. *EMBO J.* **2008**, *27*, 1172–1181.
(7) Tadokoro, T.; Kanaya, S. *FEBS J.* **2009**, *276*, 1482–1493.
(8) Cerritelli, S. M.; Crouch, R. J. *FEBS J.* **2009**, *276*, 1494–1505.
(9) Champoux, J. J.; Schultz, S. J. *FEBS J.* **2009**, *276*, 1506–1516.
(10) Schultz, S. J.; Champoux, J. J. *Virus Res.* **2008**, *134*, 86–103.
(11) Yang, W.; Hendrickson, W. A.; Crouch, R. J.; Satow, Y. *Science* **1990**, *249*, 1398–1405.
(12) Cerritelli, S. M.; Frolova, E. G.; Feng, C. G.; Grinberg, A.; Love, P. E.; Crouch, R. J. *Mol. Cell* **2003**, *11*, 807–815.
(13) Cerritelli, S. M.; Crouch, R. J. *Genomics* **1998**, *53*, 300–307.

 **10.1021/ja102933y** 

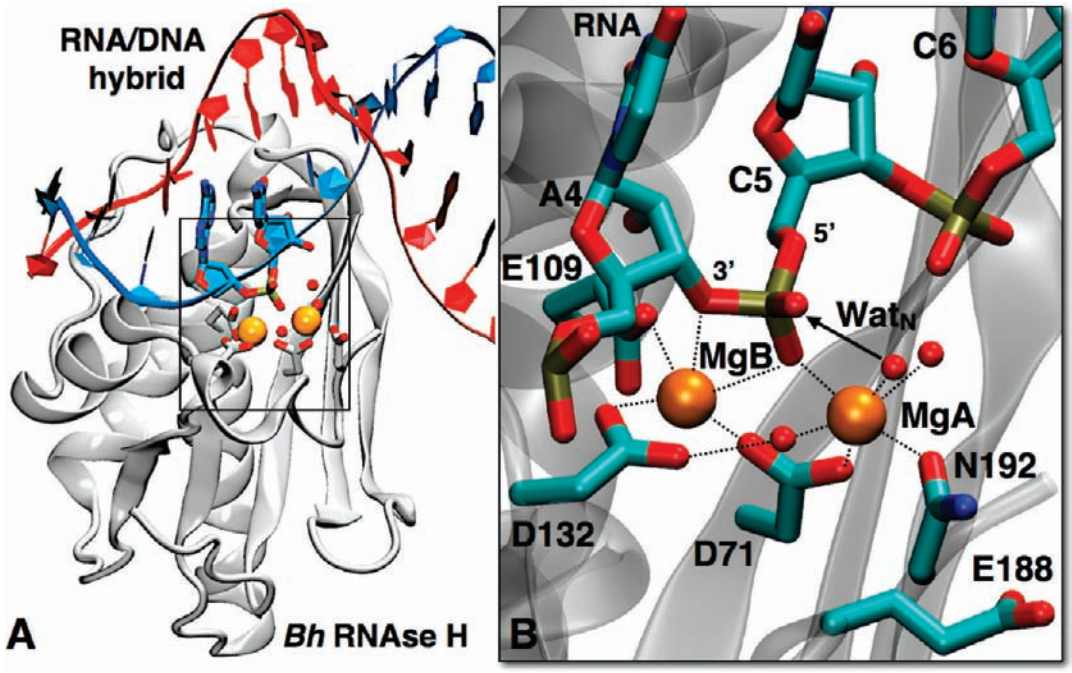


***Figure 1.*** Crystallographic structure of *Bacillus halodurans* RNase H. (A) Cartoon of the complex of RNase H and ds-RNA/DNA hybrid duplex. DNA and RNA are drawn in red and blue ribbons, respectively; orange spheres indicate the $Mg^{2+}$ ions. (B) Close-up of the catalytic site, including the RNA strand, metal ligands, and water molecules coordinated to the two crystallographic $Mg^{2+}$ ions. The key residue E188 should be noted. The D192N inactive mutant is shown (PDB code: 1ZBL).[3]

and found to be an essential enzyme in some of them. For example, RNase H knockout mice die in embryo because of the malfunction of mitochondrial DNA synthesis.[12] Malfunction of enzymes from the RNase superfamily could also result in the formation of tumors.[14] Moreover, RNase H is essential in HIV reverse transcriptase (RT)[15] and therefore is a promising target for anti-HIV drug design.[16−18] Thus, the development of ribonuclease inhibitors has drawn much attention and is an alternative strategy for anti-HIV therapies. To date, several compounds have been synthesized and showed promising results in drug discovery, such as 2-hydroxyisoquinoline-1,3(2*H*,4*H*)-dione and its derivatives.[18–20]

RNase H is a metalloenzyme that consists of a $\alpha/\beta$ fold,[3,21] with conserved carboxylate groups (i.e., DDE motif[22,23]) in the catalytic center (Figure 1). This DDE motif is essential for metal binding and catalysis. In fact, the activity of RNase H is optimal when divalent metal ions are present,[5,24] such as $Mg^{2+}$ or $Mn^{2+}$. Stereochemical[25,26] and computational[27] studies have shown that the reaction mechanism occurs via an in-line $S_N2$-like nucleophilic attack on the scissile phosphorus atom by a nucleophilic group, which is likely one hydroxyl ion in the final form, and produces 3′-hydroxyl- and 5′-phosphate-terminated products (Figure 2). Therefore, the function of the bound metal ions is both to activate the nucleophilic group by lowering its p$K_a$ value and to stabilize the formation of the transition-state structure.[28,29]

While divalent metal ions have been demonstrated to be essential for activity of the large family of riboendonucleases, their function and the exact number of bound ions in the active site[30−32] are still under debate. For example, Katayanagi et al. have proposed a single-metal-ion model according to the X-ray crystallographic analysis of *Escherichia coli* RNase HI.[33] In this model, the metal ion is bound to the RNA phosphodiester oxygen atom and three carboxyl groups. On the other hand,

(14) Kim, W.-C.; Lee, C. H. *Biochim. Biophys. Acta* **2009**, *1796*, 99–113.
(15) Hughes, S. H., Arnold, E., Hostomsky, Z. RNase H of retroviral reverse transcriptases. In *Ribonucleases H*; Crouch, R. J., Toulme, J. J., Eds.; INSERM: Paris, 1998; pp 195−224.
(16) Shaw-Reid, C. A.; Feuston, B.; Munshi, V.; Getty, K.; Krueger, J.; Hazuda, D. J.; Parniak, M. A.; Miller, M. D.; Lewis, D. *Biochemistry* **2005**, *44*, 1595–1606.
(17) Klumpp, K.; Hang, J. Q.; Rajendran, S.; Yang, Y. L.; Derosier, A.; In, P. W. K.; Overton, H.; Parkes, K. E. B.; Cammack, N.; Martin, J. A. *Nucleic Acids Res.* **2003**, *31*, 6852–6859.
(18) Klumpp, K.; Mirzadegan, T. *Curr. Pharm. Des.* **2006**, *12*, 1909–1922.
(19) Sun, W.; Pertzev, A.; Nicholson, A. W. *Nucleic Acids Res.* **2005**, *33*, 807–815.
(20) Billamboz, M.; Bailly, F.; Barreca, M. L.; De Luca, L.; Mouscadet, J. F.; Calmels, C.; Andreola, M. L.; Witvrouw, M.; Christ, F.; Debyser, Z.; Cotelle, P. *J. Med. Chem.* **2008**, *51*, 7717–7730.
(21) Nowotny, M. *EMBO Rep.* **2009**, *10*, 144–151.
(22) Kanaya, S.; Kohara, A.; Miura, Y.; Sekiguchi, A.; Iwai, S.; Inoue, H.; Ohtsuka, E.; Ikehara, M. *J. Biol. Chem.* **1990**, *265*, 4615–4621.
(23) Haren, L.; Ton-Hoang, B.; Chandler, M. *Annu. Rev. Microbiol.* **1999**, *53*, 245–281.
(24) Babu, C. S.; Dudev, T.; Casareno, R.; Cowan, J. A.; Lim, C. *J. Am. Chem. Soc.* **2003**, *125*, 9318–9328.
(25) Cassano, A. G.; Anderson, V. E.; Harris, M. E. *Biopolymers* **2004**, *73*, 110–129.
(26) Krakowiak, A.; Owczarek, A.; Koziolkiewicz, M.; Stec, W. J. *Chembiochem* **2002**, *3*, 1242–1250.
(27) De Vivo, M.; Dal Peraro, M.; Klein, M. L. *J. Am. Chem. Soc.* **2008**, *130*, 10955–10962.
(28) Steitz, T. A. *Curr. Opin. Struct. Biol.* **1993**, *3*, 31–38.
(29) Steitz, T. A.; Steitz, J. A. *Proc. Natl. Acad. Sci. U.S.A.* **1993**, *90*, 6498–6502.
(30) Strater, N.; Lipscomb, W. N.; Klabunde, T.; Krebs, B. *Angew. Chem., Int. Ed. Engl.* **1996**, *35*, 2024–2055.
(31) Pingoud, A.; Fuxreiter, M.; Pingoud, V.; Wende, W. *Cell. Mol. Life Sci.* **2005**, *62*, 685–707.
(32) Tsunaka, Y.; Takano, K.; Matsumura, H.; Yamagata, Y.; Kanaya, S. *J. Mol. Biol.* **2005**, *345*, 1171–1183.
(33) Katayanagi, K.; Ishikawa, M.; Okumura, M.; Ariyoshi, M.; Kanaya, S.; Kawano, Y.; Suzuki, M.; Tanaka, I.; Morikawa, K. *J. Biol. Chem.* **1993**, *268*, 22092–22099.

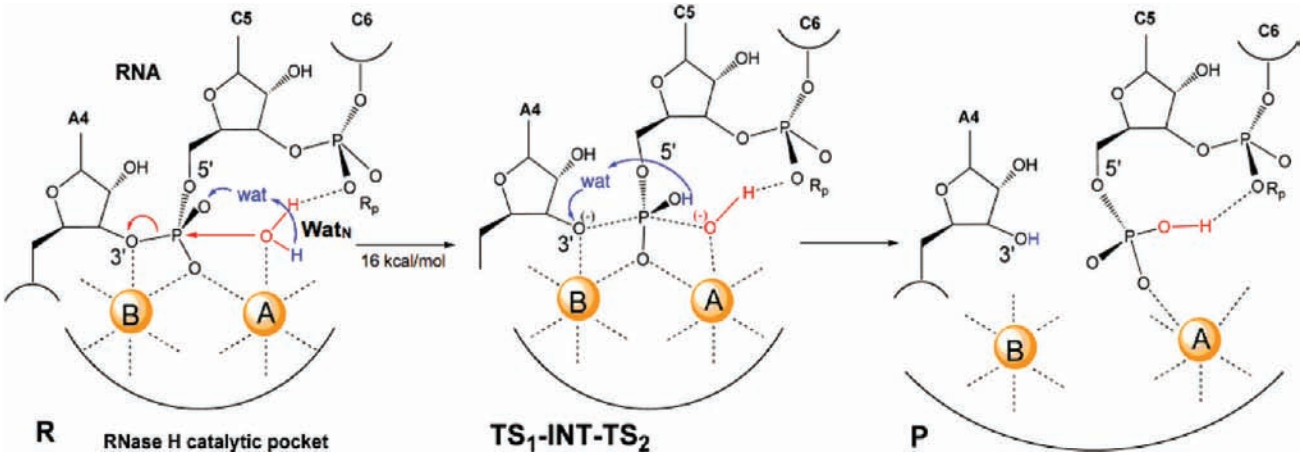


***Figure 2.*** Catalytic mechanism of RNase H as proposed by QM/MM calculations.[27] **R**: reactants state: the nucleophilic water ($Wat_N$) deprotonated *in situ* is represented in red, and the water H-bond network promoting the proton transfer to the phosphate group is shown in blue. **$TS_1$-INT-$TS_2$**: composite transition states and high-energy intermediate as calculated in previous studies.[27] **P**: product state of the cleaved RNA strand and its release from the metal site.

Smith and Pace[34] have performed kinetic analyses of RNase P and suggested that at least three metal ions are needed for optimal activity and are bound to the RNA phosphodiester group. Recently, Nowotny et al. have resolved a number of high-resolution crystal structures of RNase H from *Bacillus halodurans* (*Bh*), where two ions are situated in the catalytic pocket in complex with the substrate,[3,4] thus suggesting that a bimetal site is responsible for the catalytic activity. In particular, two $Mg^{2+}$ ions are jointly coordinated in the active site by one nonbridging oxygen atom of the scissile phosphate group of the RNA strand, four carboxylates (D71, E109, D132, and D192), and water molecules (Figure 1B). This configuration is in striking similarity to that resulting from the two-metal-ion mechanism proposed by Steitz and Steitz,[29] which suggests that one of the two metal ions activates the attacking nucleophile and the other stabilizes the formation of the transition state. This mechanism has also been suggested for other enzymes, such as Holliday junction resolvase, retroviral integrase, transposase, and RISC nuclease Argonaute.[21,35−37] For the *Bh* RNase H enzyme, we have recently investigated the enzymatic mechanism by means of DFT-based quantum mechanics/molecular mechanics (QM/MM) simulations[27] (Figure 2). Briefly, we showed how either one water molecule or one hydroxide ion can act as nucleophile, with free energy barriers of activation in good agreement with experimental data. In the case of a water molecule acting as a nucleophilic agent, water-mediated proton shuttles are involved in the water deprotonation. Importantly, we have observed the stabilization of a phosphorane intermediate during one of the possible reaction mechanisms (Figure 2). Also, the catalytic role of the two $Mg^{2+}$ ions has been shown to be critical in stabilizing the transition state.

Interestingly, it has been shown that the enzymatic activity of RNase H depends on the metal ion concentration. In fact, experiments have demonstrated that high metal concentration actually inhibits the activity of *Bh* RNase H: the activity is optimal at a $Mg^{2+}$ concentration of a few millimolar, while it is inhibited at 50 mM concentration in the gel activity assay.[3] A detailed activity study has been done for human and mouse RNase H1 up to 80 mM $Mg^{2+}$ concentration.[6] It showed that the highest activity is found at 20 mM, and activity eventually decreased at higher concentrations. In HIV RNase H, the optimal concentration is 8 mM, which is lower than that of other species.[38] These results have suggested an *attenuation effect*,[39,40] where an additional ion can influence the catalytic activity, binding to the residues near the active site—usually acidic amino acids—and eventually impairing the catalytic reaction.[39,41] For example, Marqusee et al.[39] suggested that an additional divalent metal ion could bind a carboxylate group (D134) close to the active site at high ionic concentration in *E. coli* RNase H. Consequently, a nearby histidine, which plays the role of a proton shuttle during the catalysis, is neutralized, thus losing its ability to act as a proton transporter. In *Bh* RNase H, the same inhibitory effect was observed in the gel filtration binding assay experiment, where the activity was reduced at concentrations up to 50 mM $Mg^{2+}$. This unique attenuation character is found not only in RNase H but also in other metalloenzymes. For instance, one crystal structure of the binuclear zinc cluster of LpxC reveals that a second zinc ion plays the role of an inhibitor, diminishing the catalytic activity by engaging the side chains of E78 and H265, which are a general base and an electrostatic stabilizer in the enzymatic reaction.[42] In this scenario, while it is clear that divalent metal ions are essential for the catalytic function of ribonuclease enzymes, it is not clear yet how many ions are optimal for catalysis.[31] In the case of *Bh* RNase H, Nowotny et al.[3] have proposed that E188, a glutamate residue located next to the active site (Figure 1), could recruit a third metal ion, which would help the catalytic activity through its structural and electrostatic role. In fact, E188 has shown high conformational flexibility in X-ray structures, being able to swing into and out from the active site. Also, when E188

(34) Smith, D.; Pace, N. R. *Biochemistry* **1993**, *32*, 5273–5281.
(35) Rice, P. A.; Baker, T. A. *Nat. Struct. Biol.* **2001**, *8*, 302–307.
(36) Song, J. J.; Smith, S. K.; Hannon, G. J.; Joshua-Tor, L. *Science* **2004**, *305*, 1434–1437.
(37) Yang, W.; Steitz, T. A. *Structure* **1995**, *3*, 131–134.
(38) Starnes, M. C.; Cheng, Y. C. *J. Biol. Chem.* **1989**, *264*, 7073–7084.
(39) Keck, J. L.; Goedken, E. R.; Marqusee, S. *J. Biol. Chem.* **1998**, *273*, 34128–34133.
(40) Goedken, E. R.; Marqusee, S. *J. Biol. Chem.* **2001**, *276*, 7266–7271.
(41) Oda, Y.; Yoshida, M.; Kanaya, S. *J. Biol. Chem.* **1993**, *268*, 88–92.
(42) Whittington, D. A.; Rusche, K. M.; Shin, H.; Fierke, C. A.; Christianson, D. W. *Proc. Natl. Acad. Sci. U.S.A.* **2003**, *100*, 8146–8150.

is substituted with an alanine amino acid, RNase H has a reduced activity, which is, however, retained at high metal concentrations.[3]

Here, we elucidate the nature of the catalytic metal binding site of RNase H and the role of E188 in response to different buffer concentrations. Toward this aim, we have performed a series of classical molecular dynamic (MD) simulations to study the metal−ligand coordination in *Bh* RNase H at different concentrations of $Mg^{2+}$. Importantly, we invariantly observe the presence of a third $Mg^{2+}$ ion weakly bound in the proximity of the catalytic center, chelated by the second-shell metal ligand E188. We have characterized the free energy landscape associated with conformational switches of E188 and its coordination to a third $Mg^{2+}$. Indeed, this conserved residue is able to bind the additional $Mg^{2+}$ metal ion at all the considered ionic concentrations. Remarkably, the third $Mg^{2+}$ ion does not perturb the enzymatic reactive state at standard conditions and likely tunes electrostatics for optimal catalysis. By chelating the third incoming ion, E188 prevents, in fact, a perturbation of the reactive position of the nucleophilic water molecule in the reactant state. Only when $Mg^{2+}$ concentration increases does the third $Mg^{2+}$ ion manage to displace the nucleophilic water, likely affecting the catalytic efficiency of RNase H, as seen in experiments at high $Mg^{2+}$ concentration.[3] The adapting role of E188 is confirmed by the MD simulations of the E188A mutant, which agrees with the proposed attenuation hypothesis. As a result, the present computations not only support the hypothesis that the third $Mg^{2+}$ ion is an important element in the catalytic pocket but also explain its dynamic role when coupled to E188 for modulation of RNase H activity at different ionic concentrations.

## Results and Discussion

**Conformation and Dynamics of the Active Pocket at Standard $MgCl_2$ Concentration.** A simulation at 25 mM $MgCl_2$ concentration was run to investigate the structural and dynamic features of wild-type RNase H at near-standard/optimal conditions for catalysis. The root-mean-square displacement (rmsd) value of the protein heavy atoms is 1.5 ± 0.2 Å compared to the reference crystal structure, which highlights the great stability of the enzyme framework. The DNA/RNA hybrid remained stable as well showing an average $C_1'-C_1'$ distance of 10.5 ± 0.3 Å (Figures 1 and S1, Supporting Information). The coordination shells of the two $Mg^{2+}$ ions are well preserved during the simulation (Figures 1 and 3A). In detail, **MgB** coordinates to D71, E109, D132, and the bridging ($O_3$) and nonbridging oxygen ($O_1$) atoms of the scissile phosphate of the RNA strand. The average distance of the metal to the carboxylate group is 1.90 ± 0.05 Å. The metal−RNA ligand distance is ∼2.02 ± 0.08 and ∼2.21 ± 0.14 Å for Mg−$O_1$ and Mg−$O_3$, respectively. The calculated binding distances are similar to the values observed in crystallographic magnesium carboxylate complexes[43] and QM/MM calculations.[27] The coordination geometry deviates slightly from a perfect octahedral configuration. In addition, the **MgA** coordinates to D71, D192, $O_1$ oxygen atom, and three water molecules. Specifically, the average distance of metal to the carboxylate group is 1.90 ± 0.04 Å, and it is 1.98 ± 0.07 Å for Mg−$O_1$. These structural characteristics are similar to those of the **MgB** metal−ligand coordination. One of the water molecules behaves as a bridge, connecting **MgA** and D132. Another coordinated water molecule acts as the nucleophilic group ($Wat_N$) and hydrogen bonds to the nearby pro-$R_p$ oxygen atom, forming an in-line structure with the phosphate group ($r_{O-P} \approx 3.06 \pm 0.09$ Å and $\angle_{O-P-O} \approx 167 \pm 5°$) (Figures 1B and 2). Overall, the coordination of the metal ligands for **MgA** is an ideal octahedron.

These structural determinants match well to the X-ray structures[3] and previously reported MD and QM/MM calculations[27] on the reaction mechanism. The formation of a hydrogen bond with the pro-$R_p$ oxygen atom and coordination with the metal ion are likely responsible for the p$K_a$ reduction of the attacking water molecule and its increased nucleophilicity. The role of the metal ions and the nature of the nucleophile were investigated through DFT QM/MM simulations.[27] Briefly, the two bound metal ions act cooperatively to facilitate nucleophile formation and stabilize both the transition state and the leaving group. The nucleophile formation can be achieved *in situ*, after migration of one proton from the attacking water to the scissile phosphate in the transition state. This proton shuttle is mediated by surrounding solvation water molecules, which promote the formation of a metastable phosphorane intermediate along the reaction[27] (Figure 2).

**$MgCl_2$ Concentration Does Not Affect the Conformation of the Protein and ds-DNA/RNA Hybrid Duplex.** A set of MD simulations were run using different $MgCl_2$ concentrations to test the response of the RNase H protein and the substrate DNA/RNA hybrid to different buffer conditions (from 25 to 500 mM). The relevant structural determinants of the active site are preserved regardless of counterion content (Table S2, Supporting Information). Moreover, the rmsd values of the protein heavy atoms in all the systems are similar to those in the X-ray structure (1.5 ± 0.1 Å, Figure S2, Supporting Information), and the structure of the ds-DNA/RNA substrate bound to the enzyme does not change significantly (10.6 ± 0.4 Å, measuring the length of C1′ in each base pair, Figure S1, Supporting Information). This indicates that the concentration of $MgCl_2$ does not affect the global conformation of the protein or the ds-DNA/RNA substrate, thus suggesting that the enzyme inhibition at high concentrations of $Mg^{2+}$ does not result from major conformational changes of the protein/substrate complex.

**A Third $Mg^{2+}$ Binding Site Is Adjacent to the Active Pocket and E188.** At standard $MgCl_2$ concentration, a third $Mg^{2+}$ metal ion (**MgC**) is invariantly observed in close proximity of the active site (Figure 3). This metal ion neither replaces the original bound $Mg^{2+}$ metal ions (i.e., **MgA** and **MgB**) nor significantly changes the coordination shell of the metal−ligands during the MD simulations. Interestingly, **MgC** binds to an area characterized by a high negative electrostatic potential—in particular, to E188, D192, and four water molecules—forming an octahedral coordination shell when the concentration is 25 mM (Figure 3A). This third metal binding site is likely weaker than those for **MgA** and **MgB** due to the involvement of only two protein residues and to a larger solvent-accessible area. This can explain why it was never observed in any X-ray structure so far. In fact, *B*-factors for **MgC** estimated from MD trajectories at near-standard conditions and higher $Mg^{2+}$ concentrations (see below) consistently indicate a much larger fluctuation (up to 30-fold, Table S4, Supporting Information) compared to **MgA** and **MgB**. In general, **MgC** shows high *B*-factor values (up to ∼55 Å$^2$, Table S4), which confirm its higher fluctuation.

E188 deserves special attention due to its potential effect on the RNase H activity. In fact, from the crystallographic data,[3,5] E188 was found to have great conformational flexibility. Two

(43) Harding, M. M. *Acta Crystallogr., Sect. D: Biol. Crystallogr.* **1999**, *55*, 1432–1443.

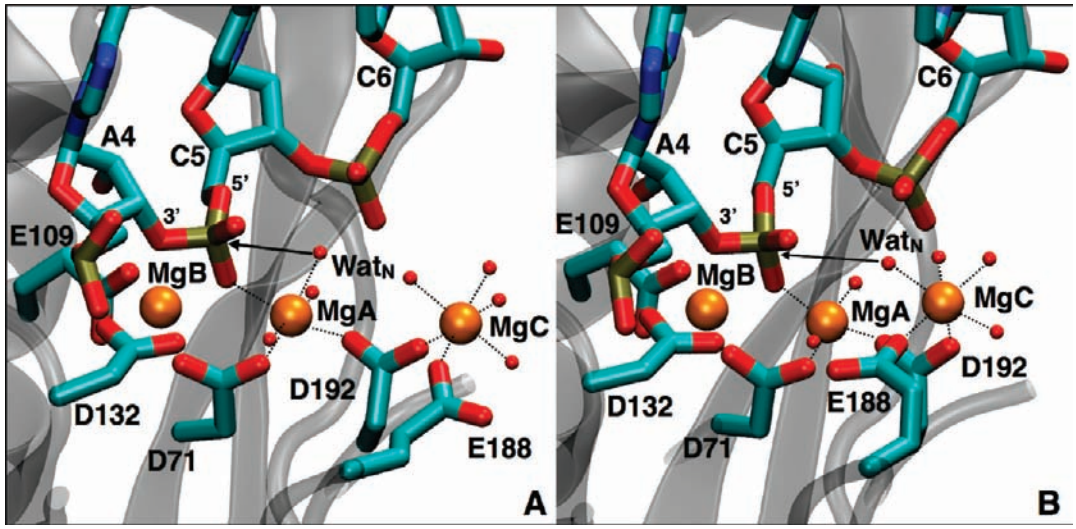


***Figure 3.*** *Active* and *inactive* states as modulated by $MgCl_2$ concentration. Two representative snapshots taken from the MD simulations show the active state (A) and the inactive state (B) dominant, respectively, at low (25 mM) and high (500 mM) $Mg^{2+}$ concentration. (A) Active state: the carboxylate group of E188 points out of the active site and $Wat_N$ binds to **MgA**. (B) Inactive state: $Wat_N$ coordinates to **MgC** and slightly loses contact with **MgA,** while the carboxylate group of E188 flips inward and points to the phosphodiester group. Metal−ligand coordination is indicated with dashed lines.

E188 conformations were found in different crystal structures of mutants (D192N and D132N) under similar conditions. In D132N, the carboxylate group of E188 points toward the active site and is 3.9 Å away from the **MgA** metal and 5.5 Å from the phosphodiester group (PDB code: 1ZBI). In D192N, on the other hand, it swings out from the active site to distances of 7.4 and 9.8 Å away from the **MgA** and phosphodiester group, respectively (Figure 1). In our MD simulation of the wild-type conformation at 25 mM $MgCl_2$ concentration, the carboxylate group of E188 stabilizes in a conformation resembling the D192N mutant, which points away from the active site (Figure 3A). Stabilization is promoted by the presence of **MgC**: in fact, in a MD simulation where additional bulk $Mg^{2+}$ ions are absent (see Supporting Information), E188 keeps swinging in and away several times, showing no preferential conformations in the nanosecond time scale (Figures S3, Supporting Information). This character might be important for the second-shell glutamate to bind divalent metals and to release the product after the chemical step.[5] Overall, this further indicates that the side chain of E188 is very flexible, and the most stable conformation of E188 is induced by the electrostatic character of the surrounding environment.

The possible existence of three $Mg^{2+}$ ion binding sites in the active pocket of endonucleases is also supported by several kinetic studies and crystallographic data.[34,44,45] Pace et al. suggested that the third metal ion binding site is located around the scissile phosphate group, and this metal ion directly participates in the catalysis in their model of RNase P. However, the **MgC** binds to a second shell residue in our simulations, and we did not observe a direct contact between the reactive species and the **MgC**. As a result, the function of **MgC** in RNase H seems not to be identical to that proposed in RNase P[34] and needs to be further investigated. Horton et al. suggested that the third $Mg^{2+}$ ion would bind to Glu45 (second shell) and Aps74 (first shell) in EcoRV and has mostly a structural role.[44,45] Finally, Nowotny et al., on the basis of mutagenesis studies of RNase H complex,[3] suggested a possible binding site around E188 due to the strong electrostatic character of the carboxylate group. However, they were unable to detect such a metal site with X-ray crystallography of mutant species at any $Mg^{2+}$ concentration, which could be explained by the high *B*-factors of the E188 carboxylate group. Thus, the present MD result supports the hypothesis of Nowotny et al. by showing the presence of a third metal ion bound to E188. Interestingly, a recent crystal structure of RNase III/ds-RNA complex presented by Ji et al. shows several $Mg^{2+}$ ions around the bimetal active site, which do not participate in the catalytic reaction. Remarkably, one of them is in a very similar position to **MgC** in our simulations, being bound to first-shell and second-shell glutamate residues[46] (see discussion and Figure 7D below).

**$MgCl_2$ Concentration Modulates the Position of the Third $Mg^{2+}$ Ion and the Catalytic Site Architecture.** The presence of **MgC** in the position adjacent to the catalytic site is confirmed by MD simulations in a broad range of $Mg^{2+}$ concentrations, namely from 25 to 500 mM $MgCl_2$. There are several metal ions bound to the phosphodiester groups of the ds-DNA/RNA strands in these systems. However, no additional $Mg^{2+}$ ions are found within a sphere of ∼12 Å radius around the active site at any $MgCl_2$ concentration (Figures 4A), apart from the **MgA**, **MgB**, and **MgC**. Thus, regardless of the $MgCl_2$ concentration, the third magnesium ion seems to have a preferential electrostatic binding pocket close to the active site, involving first- (D192) and second-shell (E188) metal ligands.

Importantly, two preferential binding modes are observed for **MgC**, which are regulated by $Mg^{2+}$ concentration and determine the position of the flexible residue E188 (Figure 3). One stable conformation is that found at 25 mM, where E188 binds to the third ion, which however does not perturb the catalytic site and likely leads to the optimal catalytic activity.[27] This state is hereafter referred to as the *active* state, meaning that the nucleophilic $Wat_N$ binds strongly to **MgA** (2.1 Å, Table S2, Supporting Information) and represents a reactive Michaelis complex (Figure 3A). In the second conformation E188 is no

(44) Horton, N. C.; Perona, J. J. *Biochemistry* **2004**, *43*, 6841–6857.
(45) Horton, N. C.; Connolly, B. A.; Perona, J. J. *J. Am. Chem. Soc.* **2000**, *122*, 3314–3324.
(46) Gan, J.; Shaw, G.; Tropea, J. E.; Waugh, D. S.; Court, D. L.; Ji, X. *Mol. Microbiol.* **2008**, *67*, 143–154.

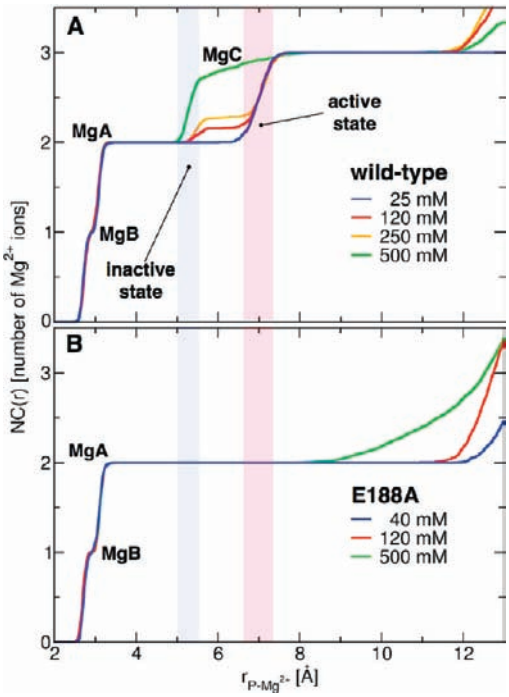


***Figure 4.*** $Mg^{2+}$ distribution at the active site of RNase H. The number of coordinated $Mg^{2+}$ ions (NC) around the C5 phosphodiester P atom is shown as extracted from the MD simulations of wild-type (A) and E188A-mutated system (B) at different $MgCl_2$ concentration. NC(r) is derived from the integration of the P−$Mg^{2+}$ radial distribution function. The localization of **MgC** in the *active* and *inactive* states is shown by the blue and red areas, respectively (Figure 3).

longer able to protect the optimal catalytic structure, and the third ion disrupts the nucleophilic water orientation: this conformation is hereafter referred to as the *inactive* state, meaning that the nucleophilic group binds more strongly to **MgC** than **MgA** (Figure 3B, Table S2).

The long, solvent-exposed side chain of E188 is able to chelate the third $Mg^{2+}$ ion at normal concentration (i.e., 25 mM) and to maintain this third metal at a distance from the catalytic site which is optimal for the catalytic mechanism. We propose that the presence of **MgC** can be important for the correct modulation of the catalytic reaction. At higher concentrations (e.g., 250 and 500 mM), the third $Mg^{2+}$ and its coordination shell are pushed closer to the catalytic site due to the higher electrostatic repulsion of the buffer (Figures 3B and 4A; Figure S7 and Table S2, Supporting Information). In this inactive conformation, **MgC** and **MgA** are closer to each other, at a distance of ∼4.5 Å. As a consequence, to compensate the strong charge−charge repulsion, **MgA** shifts slightly and moves toward **MgB**, producing frustration at the active site (**MgA**−**MgB** distance is ∼3.4 Å, Table S2). The distance separating **MgC** and **P** is ∼5.4 Å.

Most importantly, the **MgA** metal ion loses the coordination with the nucleophilic water ($Wat_N$) and forms a distorted octahedral geometry (Figure 3B). $Wat_N$ moves away and coordinates to **MgC** while still forming a hydrogen bond with the pro-$R_p$ oxygen. The distance to **P** becomes longer (∼3.5 Å), and the value of the angle $Wat_N$−P−$O_3$ becomes smaller (∼153.0°). Moreover, the position of **MgC** does not allow for the insertion of an additional water molecule, which would repair the coordination shell of **MgA** and act as a reactive nucleophile. All this leads to an unfavorable conformation of the nucleophilic group, which is distorted compared to the active reactant state (Figure 3B).

While the inactive conformation remains stable at high concentrations (250 and 500 mM), it is also observed at lower concentrations. However, it is only transient at lower $MgCl_2$ concentrations (from 25 to 100 mM), likely biased by the initial starting conformation, and structural changes rapidly occurring after a few nanoseconds of MD lead to an equilibrated conformation in which the third $Mg^{2+}$ ion does not significantly perturb the reactants state, as found in previous MD simulations[27] (Figure 3A). [Interestingly, the observed transition time to pass from a catalytic-perturbed conformation to an active conformation increases with the concentration of $Mg^{2+}$ ions. Specifically, the transition time is less than 1 ns in the system with 25 mM $Mg^{2+}$, ∼6 ns at 100 mM, ∼8 ns at 250 mM, and ∼16 ns at 500 mM, which is consistent with MgC radial occupancy reported in Figure 4A.]

The orientation of E188 is correlated to the position of **MgC**. In the active state, the E188 carboxylate group mostly points away from the active site (Figure 3A). The dihedral angle ($C_\alpha$−$C_\beta$−$C_\gamma$−$C_\delta$) of the side chain on E188 reflects the two states explored by free MD. The angle is ∼ −90° and ∼ −180° in the inactive state and in the active state, respectively (Figures 3 and S3, Supporting Information). It is worth mentioning that the dihedral angle of the active conformation for E188 is identical to the one in the D192N X-ray structure.

Overall, two conformations of the active site are observed, which are clearly related to the position of **MgC** and its ligands E188 and D192. The **MgB** site retains its coordination geometry in both states, indicating that its coordination shell is very stable and is not affected by the appearance of an extra metal ion. On the other hand, the coordination geometry of the **MgA** site is correlated to the binding position of **MgC**, and it can be largely affected along with the position of the nucleophilic $Wat_N$. From the conformational space sampled through free MD simulations, we can confidently state that, at normal concentration of $MgCl_2$, the inactive state is not stable. However, at higher concentration of $MgCl_2$ the inactive state becomes more and more predominant, likely producing a significant perturbation of the optimal catalytic site architecture.

**How $MgCl_2$ Concentration and Third $Mg^{2+}$ Position Affect the Catalytic Mechanism.** The MD simulations reveal two distinct conformations, and yet it is not easy to determine the most stable structure without a very long MD trajectory. Hence, we performed free energy calculations using the Adapting Biasing Force (ABF) method[47] to study how the free energy surface is affected by $MgCl_2$ concentration.

A first reaction coordinate ($RC_1$) is chosen as the distance separating the **P** and **MgC** (Figure 5A). In other words, $RC_1$ describes the free energy surface (FES) related to the vicinity of **MgC** on the reactive center. Free energy profiles for systems at low and high concentration (i.e., 25 and 500 mM, respectively) are shown in Figure 5A. The minimum of the FES at 25 mM is at $RC_1$ = 7.1 Å, which shows structural determinants identical to those observed in the active state at 25 mM of free MD runs. Another, shallower minimum is located at 5.2 Å < $RC_1$ < 5.7 Å, which is consistent with the position of the inactive state. Therefore, the ABF calculation clearly describes the two-state conformation behavior of **MgC** as found in the free MD simulations. The free energy of the inactive state is 5 kcal/mol

(47) Henin, J.; Chipot, C. *J. Chem. Phys.* **2004**, *121*, 2904–2914.

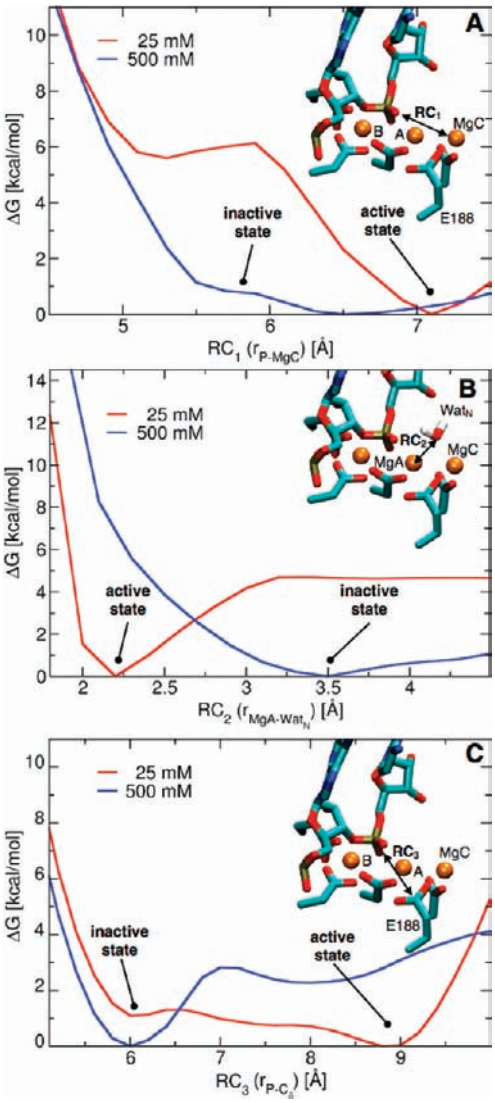


***Figure 5.*** Free energy landscape of the active-site architecture at low and high $MgCl_2$ concentration. The free energy surface at 25 (red) and 500 mM (blue) $MgCl_2$ as a function of the **MgC**-to-phosphodiester group phosphorus atom (**P**) separation, $RC_1$ (A); the **MgA**-$Wat_N$ separation, $RC_2$ (B); and the E188-to-phosphodiester group distance, $RC_3$ (C). The reaction coordinate $RC_3$ is chosen as the distance that separates the carboxylate group ($C_\delta$) of E188 and the phosphorus atom (P). Insets represent graphically the reaction coordinates adopted in ABF calculations.

higher than that of the active state, which implies an occupation ratio of 1:4400 for these conformations at 300 K. This also points to a large instability for the inactive state at low $Mg^{2+}$ concentration. Importantly, at standard conditions, **MgC** has a preferential pocket at the active site that likely serves to optimally tune the electrostatics of the reactants state. The FES shows a different character at 500 mM $Mg^{2+}$ concentration. The global minimum is located at $RC_1 = 6.5$ Å, which is 0.6 Å closer to the active state than at low $Mg^{2+}$ concentration. It is also broader, spanning from 6.0 to 7.0 Å, which could result from the loosely binding configuration of **MgC** with only one ligand (E188) at 500 mM $Mg^{2+}$. A second minimum is found at 5.7 Å, which corresponds to the configuration of the inactive state. The free energy difference between these two conformations is less than 1.0 kcal/mol at high $Mg^{2+}$ concentration, which indicates that the probability of finding these two conformations is almost equal at 300 K. As a result, the inactive state is more stable at higher $Mg^{2+}$ concentration, pointing to a crucial role of the third metal for the inhibition of the chemical step, as shown by experiments.[3]

As shown above, the inactive state leads to an unfavorable conformation of the nucleophilic group, which is distorted compared to the active reactant state (Figure 3B). This suggests that the nucleophilic propensity of the $Wat_N$ would likely be decreased and explains the diminished catalytic activity at high concentration. Free energy calculations exploring the MgA−$Wat_N$ reaction coordinate ($RC_2$) indicate, in fact, that $Wat_N$ steadily binds to **MgA** in the active state (2.2 Å, Figure 5B). On the other hand, $Wat_N$ prefers to bind to **MgC** in the inactive state at 500 mM (3.5 Å), and it takes ∼6.7 kcal/mol to bring $Wat_N$ closer to **MgA** (i.e., at 2.2 Å) in an optimal position for the nucleophilic attack, as observed in previous QM/MM studies[27] (Figure 5B).

Moreover, E188 plays a crucial role in regulating this mechanism: it chelates and screens **MgC**, modulating its binding position at different $Mg^{2+}$ concentrations thanks to the flexibility of its side chain (Figure 3). For example, the average distance between the E188 carboxylate group and **P** is 5.6 ± 0.2 Å in the inactive state and 8.5 ± 0.8 Å in the active state. A sampling of the free energy landscape associated with this distance at 25 and 500 mM $MgCl_2$ concentrations showed that the equilibrium distance of E188 is related to the ionic concentration (Figures 5C and S6, Supporting Information). This degree of freedom is sampled using the reaction coordinate $RC_3$, which describes the FES related to the conformational change of the E188. At low concentration (25 mM), the energy minimum is located at ∼8.8 Å (with second minimum at 6.0 Å), similar to the conformation of the active state (Figure 3A). It is worth pointing out that this conformation is also similar to the X-ray structure, in which D192 is mutated to N192 (Figure 1B). The energy barrier is very small, about 1.5 kcal/mol. The energy minimum shifts to 6.0 Å at 500 mM concentration. A shallow minimum was found at 8.0 Å. Moreover, the energy barrier increases to 3.0 kcal/mol. This suggests that the inactive state is more stable at high concentration of $MgCl_2$, in agreement with the previous free energy calculations (Figure 5A).

In summary, at normal $MgCl_2$ concentrations, E188 binds to the third $Mg^{2+}$ ion, which is naturally attracted in the solvent-exposed pocket around the active metal center. The most favorable conformation obtained by the free energy exploration of the active-site architecture is the one that preserves a reactive conformation of the nucleophilic water (Figure 3A). Conversely, at high concentrations, the **MgA** coordination shell is distorted when **MgC** gets closer, and the nucleophile directly binds to **MgC**, disrupting its optimal orientation for the nucleophilic attack (Figures 3B and 5B).

**Rationalization of the Attenuation Effect in RNase H.** Both the free energy calculations and free MD simulations revealed the importance of E188 in the second shell of metal ligands and suggested that the dynamics of this amino acid could be important for explaining the *attenuation effect*.[39,40] Since RNase systems are extremely sensitive to metals and are inhibited by high $Mg^{2+}$ concentrations, many studies have been done to address this question. A possible explanation for the attenuation effect is the existence of multiple metal binding sites in the active site. Electrostatic potential calculation[48] shows that the area around D192 and E188 possesses a high negative electrostatic potential (Figure 6A) and thus indicates, consistent with

(48) Baker, N. A.; Sept, D.; Joseph, S.; Holst, M. J.; McCammon, J. A. *Proc. Natl. Acad. Sci. U.S.A.* **2001**, *98*, 10037–10041.

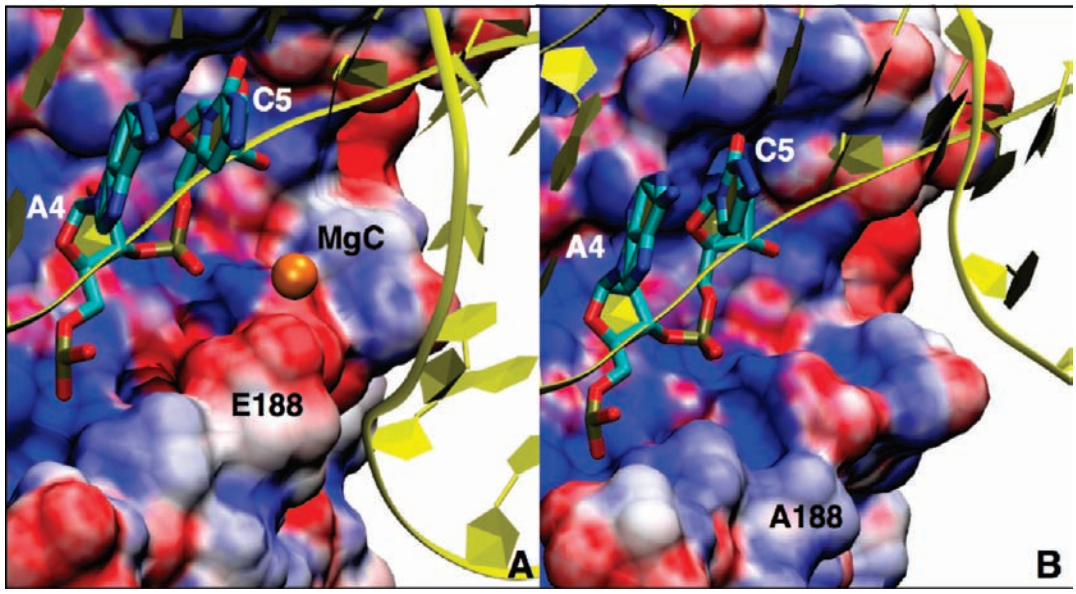


***Figure 6.*** Calculated electrostatic properties of the active site in RNase H. Shown are electrostatic potentials (ESPs) obtained using the adaptive Poisson−Boltzmann solver method with dielectric constants of 1.0 and 78.5 for the solute and solvent, respectively (color scale: +10 (blue) and −10 kT/e (red)). The RNA/DNA hybrid is represented as a yellow ribbon. The calculated ESP for the wild-type system (A) and for the E188A mutant (B) is mapped on the protein molecular surface. Position 188 in both systems is indicated by residue labels; the orange sphere represents the location of the third $Mg^{2+}$ ion.

previous calculations reported in this work, that E188 defines an additional metal binding site, besides the DDE motif in the RNase H. Therefore, the removal of this glutamate group can reduce the propensity of attracting the third metal ion, which is likely needed for optimal catalysis, as emerged from our simulations.

This hypothesis was further tested by performing MD simulations of a mutated E188A system, which is known to show a reduced activity *in vitro* with respect to the wild-type.[3] During MD simulations, the metal ions **MgA** and **MgB** maintain their coordination geometry very well, and the overall structural determinants are always identical at different $Mg^{2+}$ concentrations. These results are in agreement with what was observed in mutagenesis experiments of E188A, where activity is always retained at any buffer concentration,[3] despite showing a reduction compared to the wild-type enzyme. Strikingly, we did not observe in MD at any $MgCl_2$ concentration a third $Mg^{2+}$ bound to the third metal site found in the wild-type. In fact, apart from the two metal ions bound at the active site, no other $Mg^{2+}$ ions were found within ∼10 Å from **P**, based on the calculation of the radial distribution function (Figure 4B). In addition, the original negative electrostatic character, calculated on the basis of the Poisson−Boltzmann equation around E188, is not shown in the E188A system (Figure 6B). Thus, the E188A mutant does not produce a favorable third metal binding site, regardless of the $MgCl_2$ concentration. Any structural feature along with the solvation structure around the metal active site is identical in the wild-type and E188A system apart the presence of the third $Mg^{2+}$ metal. Importantly, the nucleophilic $Wat_N$ is not perturbed at any concentration and always has the canonical conformation found in the active state of the reactants (Table S2, Supporting Information). This strongly supports the hypothesis that the third $Mg^{2+}$ metal is indeed important for the optimal tuning of the reaction: it is the only distinctive difference that emerged from MD simulations that can explain the reduced catalytic activity shown by E188A mutants.[3] The removal of E188 not only could compromise the $Mg^{2+}$ ion loading on the active site but also perturbs the electrostatic field during turnover, leading to an unfavorable electrostatic environment for catalysis and the dissociation and release of the products.[5]

While E188 clearly shows its ability to bind to solvated divalent ions, the catalytic role of **MgC** is still not fully understood. Nowotny et al.[3] proposed that E188 can bind to **MgA** and promote the product leaving. However, the observation of **MgC** in our MD simulations suggests that the role of **MgA** can be replaced by this third bound metal ion. An X-ray structure of the product state (PDB code: 2G8V) shows **MgA** still bound to the active site, suggesting that the products leave the active site without the dissociation of **MgA**. As a result, we propose that **MgC** could bind to the product after the catalysis and promote the dissociation of the hydrolyzed RNA strand. In this scenario, the third $Mg^{2+}$ ion, at normal concentrations (as found in MD simulations of wild-type), can be functional by enabling the efficient progress of the catalytic reaction. Without its presence (i.e., in the E188A system) the reaction progresses anyway but with reduced activity. A more quantitative estimation of the catalytic contribution of the third ion upon change in concentration will be assessed by QM/MM simulations that are currently in progress.

**A Three-Metal Binding Site Can Be a Recurrent Motif in the Endonuclease Family.** The occurrence of a third and more mobile metal ion at the catalytic site, and coordinated by second-shell Glu/Asp residues, could in principle be functional not only in the *Bacillus halodurans* RNase H system but also in other similar proteins. A search in the structure database showed that second-shell glutamate residues are found in several NT superfamily enzymes (Figure 7). For example, a glutamate group (E131) is found in the second shell of *E. coli* RNase H[40] (PDB code: 1G15, Figure 7B), which with D134 could define a similar third metal site as in *Bh* RNase H. Supporting this hypothesis is the fact that also *E. coli* RNase H shows the attenuation effect.[39,40] In prokaryotic DNA transposase[49] (Tn5, PDB code:

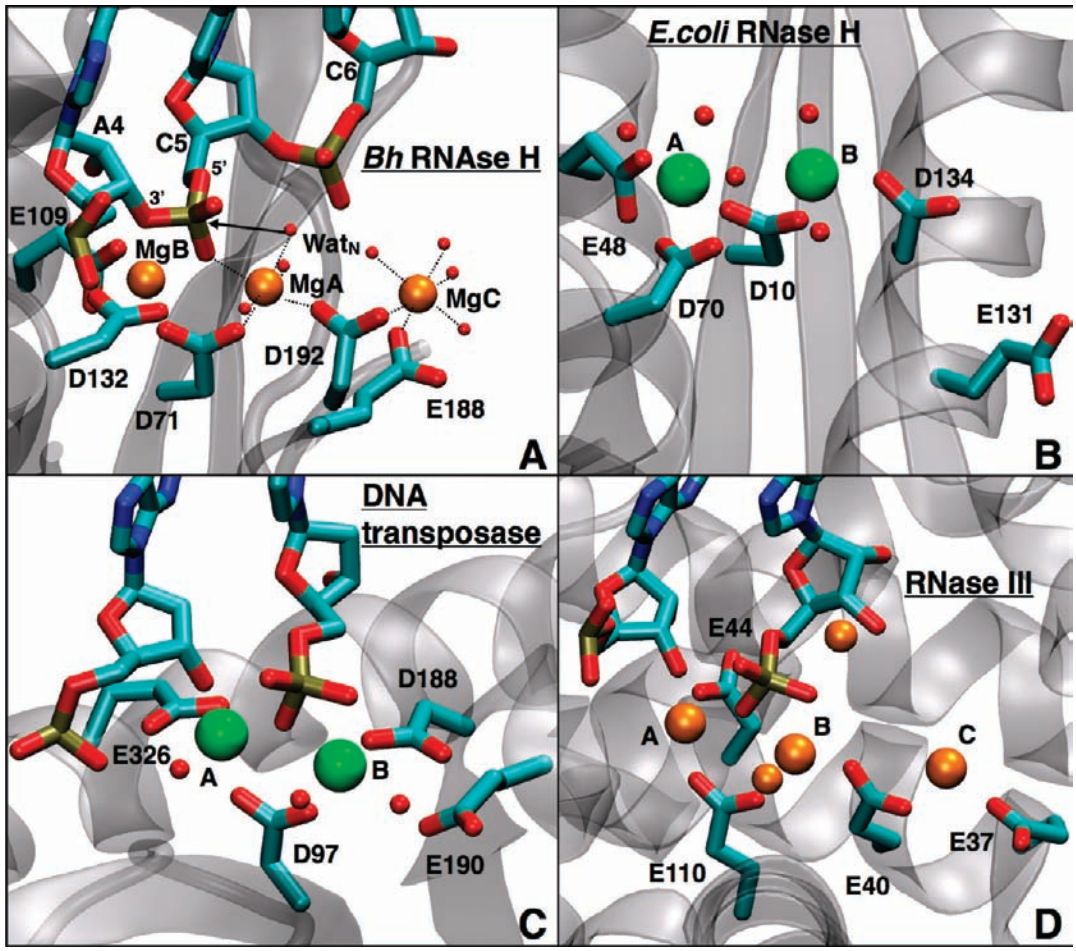


***Figure 7.*** Active sites of other members of the NT superfamily showing a second-shell glutamate residue. (A) The active conformation from the present work on *Bh* RNase H; (B) E. *coli* RNase H X-ray structure (PDB code: 1G15); (C) prokaryotic DNA transposase (PDB code: 1MUS); (D) Aa-RNase III/ds-RNA complex (PDB code: 2NUG). HIV reverse transcriptase (PDB code: 1SUQ) also shows this motif (structure not shown). Magnesium ions are represented as orange spheres, manganese ions as green spheres. Divalent ions that superimpose to **MgA**, **MgB**, and **MgC** in the present work are labeled specifically.

1MUS, Figure 7C), a glutamate group (E190) is found 6.8 Å away from the active site. A second-shell ligand glutamate residue E478 is also found in the mononuclear HIV reverse transcriptase[50] (PDB code: 1SUQ) and might have a similar role in recruiting additional metal ions at the active site. Recently, an Aa-RNase III/-RNA complex has been presented, and for the first time more than two metal ions have been observed at the active site of an endonuclease.[46] A total of five $Mg^{2+}$ ions have been indeed resolved (PDB code: 2NUG, Figure 7D); importantly, apart from the two main catalytic $Mg^{2+}$ ions (**MgA** and **MgB** in *Bh* RNase H) that hold the phosphodiester group to be cleaved, one metal ion can be clearly spatially compared to **MgC** in RNase H, being directly coordinated to two glutamate residues, E40 and E37, which correspond to D192 and E188 in *Bh* RNase H. The distance between this $Mg^{2+}$ metal and P is ~7 Å, similar to the arrangement obtained from MD simulation for active-state conformation. Although representing a product state for RNase III, this structure points to the existence of additional metal binding sites in the endonuclease catalytic pocket and, together with our present computational results for *Bh* RNase H, suggests a more complex metal modulation in endonuclease catalysis. In general, the presence of additional acidic amino acids in the second shell implies that they could have a role for binding metal ions to the catalytic site and for optimally tuning the catalytic pocket electrostatics.

## Conclusions

RNase H has become a popular target because of its critical role in many biological processes, involved in the RNA degradation of ds-DNA/RNA hybrid duplex. Also, a recent crystallographic study of the influenza A polymerase[51] reveals a similar structure of the active site, with two-metal ions bound at the DDE motif. This indicates that a comprehensive study of the structural determinants of the RNase family might be beneficial to drug discovery projects targeting other endonucleases, which share a similar two-divalent-metal catalytic mechanism. Numerous crystallographic and spectroscopic studies have been performed for RNase H and attempted to unravel the reaction mechanism. Experimental data and theoretical calculations[27,52] suggest a two-divalent-metal-aided $S_N2$-like mechanism. However, the cause of the attenuation effect, by

(49) Steiniger-White, M.; Rayment, I.; Reznikoff, W. S. *Curr. Opin. Struct. Biol.* **2004**, *14*, 50–57.
(50) Das, K.; et al. *J. Med. Chem.* **2004**, *47*, 2550–2560.
(51) Dias, A.; Bouvier, D.; Crepin, T.; McCarthy, A. A.; Hart, D. J.; Baudin, F.; Cusack, S.; Ruigrok, R. W. H. *Nature* **2009**, *458*, 914–918.
(52) Rosta, E.; Woodcock, H. L.; Brooks, B. R.; Hummer, G. *J. Comp. Chem.* **2009**, *30*, 1634–1641.

which the RNase H activity is perturbed at high concentrations of divalent metal ions, is still unclear. In this article, we have presented an investigation of the structure of the RNase H active site using MD with empirical force fields. In addition, ABF calculations have been performed to determine the free energy landscape associated with conformational changes in the active site and to understand the role of conserved second-shell metal ligands (E188) related to the concentration of solvated metal ions.

The present calculations indicate that, in addition to the originally known two metal ions bound at the active site, there is an extra metal. At low $Mg^{2+}$ concentrations, this third metal ion binds to D192 and E188 and is ~7.0 Å away from the scissile phosphate group. Conversely, at high $Mg^{2+}$ concentrations, the stronger electrostatic influence of the buffer brings the third metal ion and its coordination sphere closer to the catalytic site. Importantly, this seems to lead to an inactive conformation of the catalytic site, where the nucleophilic water molecule is displaced from its optimal position for catalysis (Figure 3). The free energy calculations show that this inactive conformation is more stable at higher $Mg^{2+}$ concentrations (Figure 5), at which the nucleophilic water molecule is more distant from the scissile group. It has been shown that the free energy cost to bring the nucleophilic water close to the optimal reactive state is higher at higher concentrations (Figure 5B), explaining the inhibitory effect of the high concentration of metal ions. Moreover, the mutated E188A RNase H system, which presents a weaker but conserved activity at any $MgCl_2$ concentration, shows that the third metal ion does not bind to the active site at any ionic concentration, pointing to a crucial catalytic role at standard conditions of the third $Mg^{2+}$ metal coordinated to the acidic second-shell residue, E188.

The presence of glutamate residues in the second-shell ligand layer in other endonuclease enzymes (Figure 7) might also suggest the functional conservation of this structural motif, which can optimally and flexibly modulate the RNA phosphodiester cleavage. Ultimately, these results could inspire the structure-based design of modulators/inhibitors that target the principal metal binding site along with the third site and its structural coupling to the acidic second-shell residue. Molecules could be designed in order to probe catalytic activity and/or inhibition with linkers connecting these two sites, which exploit the concentration-dependent distance observed between the metal sites. Alternatively, the endonuclease activity could be modulated by engineering specific mutations affecting the third metal binding site. This could be the case for several endonucleases with second-shell carboxyl ligands that use a structural triad of divalent ions to favor metal uptake and electrostatic modulation of the catalytic turnover.

## Materials and Methods

**Structural Models.** A model of the *Bacillus halodurans* RNase H and ds-DNA/RNA 12-mer complex was generated on the basis of the X-ray structure reported by Nowotny et al. (PDB code: 1ZBL, 2.2 Å resolution, Figure 1),[3] which is a D192N mutant enzyme with completely impaired activity. In this inactive enzyme, the active-site architecture does not significantly change from the wild-type system. Thus, N192 is substituted by an aspartic acid to reproduce the wild-type sequence. Two bound metal ions found in the active site are conserved (**MgA** and **MgB**). For the MD simulations, a total of five enzyme−substrate adducts were generated with different $MgCl_2$ concentrations. Each system was immersed in a 65 Å × 73 Å × 76 Å rectangular water box; ~11 000 TIP3P water molecules were needed to solvate the system. $Mg^{2+}$ and $Cl^-$ ions were used as counterions to provide the target concentration in the five different MD runs. Specifically, in addition to the counterions needed to neutralize the system, extra solvated $Mg^{2+}$ ions were added, respectively 3, 22, 50, and 100. The corresponding $MgCl_2$ concentrations are estimated to be approximately 25, 120, 250, and 500 mM, respectively, where 25 mM is the condition closer to standard/optimal concentration for RNase H. In order to investigate the inhibitory effect of E188, a mutated system was generated by replacing the glutamate residue by an alanine. Various concentrations of $MgCl_2$ were used to prepare the E188A system (40, 120, and 500 mM $MgCl_2$). Due to the limited simulation cell size and the necessity to neutralize the system in periodic boundary conditions, the computed $Mg^{2+}$ concentration is influenced by the protein volume. In addition, the ratio between the solvated divalent metal ions and the enzyme in the simulation is much smaller than in the experiment setup, which is millimolar in $Mg^{2+}$ vs picomolar in the case of the RNase H enzyme.[6] Nevertheless, the results from the present study are likely to be indicative of a quantitative trend for relevant structural and dynamic properties of the active site when passing from low to very high concentrations of $Mg^{2+}$ ions.

**Molecular Dynamics.** The AMBER force field (parm99sb)[53,54] was adopted for all standard residues and nucleic acids. The metal active site is treated with a flexible nonbonded approach based on the "atoms in molecules" partitioning scheme of the DFT-BLYP level electronic density of the active site, as explained in detail in ref 55. This allows one to account for the metal−ligand interactions and permits possible structural rearrangements at the active site during the MD simulations. Specifically, Bader's atomic charges were used for the two $Mg^{2+}$ ions and their ligands in the active site (D71, E109, D132, D192, and phosphodiester group on the substrate RNA strand). Aqvist's parameters for solvated $Mg^{2+}$ ion were adopted for the remaining $Mg^{2+}$ ions.[56] More details on the MD setup procedure and the Bader atomic charges are reported in the Supporting Information. All the simulations were performed with the NAMD package.[57] A total of 20 ns of dynamics was performed for all the systems, and the last 16 ns of trajectory was used for data analysis.

**Free Energy Calculations.** To investigate the effects due to the conformational changes of the active site after the binding of the third $Mg^{2+}$ ion at different concentration, we performed unconstrained MD simulations in the NPT ensemble to compute the free energy surface (FES) derived from the potential of mean force (PMF), using the Adaptive Biasing Force (ABF) method.[47] In brief, the PMF, or the derivative of the Gibbs free energy ($G$) along the defined reaction coordinate (RC, $\xi$), $dG/d\xi$, is computed as

$$\frac{dG}{d\xi} = -\left\langle \frac{d}{dt}\left[\left(\sum_i \frac{1}{m_i}\left(\frac{\partial \xi}{\partial x_i}\right)^2\right)^{-1} \frac{d\xi}{dt}\right]\right\rangle_\xi$$

Here, $m_i$ is the mass of atom $i$, $x_i$ is the Cartesian coordinate of atom $i$, and $t$ is time variable. The Gibbs free energy, in this case, is acquired from the integration of the PMF:

$$G(\xi) = -\int \langle \frac{dG}{d\xi} \rangle_\xi \, d\xi$$

A detailed description of this method can be found in ref 47.

(53) Cornell, W. D.; Cieplak, P.; Bayly, C. I.; Gould, I. R.; Merz, K. M.; Ferguson, D. M.; Spellmeyer, D. C.; Fox, T.; Caldwell, J. W.; Kollman, P. A. *J. Am. Chem. Soc.* **1995**, *117*, 5179–5197.
(54) Hornak, V.; Abel, R.; Okur, A.; Strockbine, B.; Roitberg, A.; Simmerling, C. *Proteins*, **65**, 712–725.
(55) Dal Peraro, M.; Spiegel, K.; Lamoureux, G.; De Vivo, M.; DeGrado, W. F.; Klein, M. L. *J. Struct. Biol.* **2007**, *157* (3), 444–453.
(56) Aqvist, J. *J. Phys. Chem.* **1990**, *94*, 8021–8024.
(57) Phillips, J. C.; Braun, R.; Wang, W.; Gumbart, J.; Tajkhorshid, E.; Villa, E.; Chipot, C.; Skeel, R. D.; Kale, L.; Schulten, K. *J. Comput. Chem.* **2005**, *26*, 1781–1802.

Three reaction coordinates for ABF calculations have been used to describe the FES associated with conformational changes of the active site upon third ion binding (Figure 5): (1) The distance $RC_1$, which separates the third bound $Mg^{2+}$ ion (**MgC**) and the C5 phosphodiester phosphorus atom P. $RC_1$ describes the FES related to the effect of the vicinity of **MgC** to the reactive center of the active site. The boundary of $RC_1$ is set as 4.9 Å < $RC_1$ < 7.5 Å (Figures 5A). (2) $RC_2$, defined as the distance between **MgA** and $Wat_N$, which explores the concentration-dependent nucleophilic character of $Wat_N$. The boundary of $RC_2$ is set to 1.5 Å < $RC_2$ < 4.5 Å (Figure 5B). (3) The distance $RC_3$, separating the carboxylate group ($C_\delta$) of E188 and the P atom (Figures 5C). $RC_3$ describes the FES related to the conformational change of the E188. For all calculations, the instantaneous values of the force were accrued in bins 0.2 Å wide. For each calculation, the trajectory of the system is monitored to make sure the system is well sampled along the reaction coordinate and that the variation of the computed free energy over a 2 ns windows is less than 0.1 kcal/mol (Figures S5 and S6, Supporting Information).

**Acknowledgment.** We thank Prof. Allen Nicholson and Dr. Jérôme Hénin for their interest and useful discussions. This research was supported in part by the NIH under grant GM 067689 with computational resources provided by TeraGrid.

**Note Added after ASAP Publication.** The uncorrected proof version of this article was published ASAP August 23, 2010. The fully corrected version, with changes in the text and references, was published September 15, 2010.

**Supporting Information Available:** Additional results, tables, and figures; complete ref 50. This material is available free of charge via the Internet at http://pubs.acs.org.

JA102933Y